Does the spatial arrangement of urban landscape matter? examples of urban warming and cooling in phoenix and las vegas

Soe Win Myint, Baojuan Zheng, Emily Talen, Chao Fan, Shai Kaplan, Ariane Middel, Martin Smith, Huei-ping Huang & Anthony Brazel

Does the spatial arrangement of urban landscape matter? Examples of urban warming and cooling in Phoenix and Las Vegas

Soe Win Myint,[1,6] Baojuan Zheng,[1,2] Emily Talen,[1] Chao Fan,[1] Shai Kaplan,[1,3] Ariane Middel,[1,4] Martin Smith,[4] Huei-Ping Huang,[5] and Anthony Brazel[1]

[1]School of Geographical Sciences and Urban Planning, Arizona State University, 975 South Myrtle Avenue, Tempe, Arizona 85287 USA
[2]Geospatial Sciences Center of Excellence, South Dakota State University, 1021 Medary Avenue, Wecota Hall 115, Box 506B, Brookings, South Dakota 57007 USA
[3]Department of Geography and Environmental Development, Ben-Gurion University of the Negev, P.O. Box 653, Beer-Sheva 8410501 Israel
[4]School of Sustainability, Arizona State University, Wrigley Hall, 800 Cady Mall 108, Tempe, Arizona 85281 USA
[5]School for Engineering of Matter, Transport, and Energy, Arizona State University, 501 East Tyler Mall, P.O. Box 876106, Tempe, Arizona 85287 USA

Abstract. This study examines the impact of spatial landscape configuration (e.g., clustered, dispersed) on land-surface temperatures (LST) over Phoenix, Arizona, and Las Vegas, Nevada, USA. We classified detailed land-cover types via object-based image analysis (OBIA) using Geoeye-1 at 3-m resolution (Las Vegas) and QuickBird at 2.4-m resolution (Phoenix). Spatial autocorrelation (local Moran's I) was then used to test for spatial dependence and to determine how clustered or dispersed points were arranged. Next, we used Advanced Spaceborne Thermal Emission and Reflection Radiometer (ASTER) data acquired over Phoenix (daytime on 10 June and nighttime on 17 October 2011) and Las Vegas (daytime on 6 July and nighttime on 27 August 2005) to examine day- and nighttime LST with regard to the spatial arrangement of anthropogenic and vegetation features. Local Moran's I values of each land-cover type were spatially correlated to surface temperature. The spatial configuration of grass and trees shows strong negative correlations with LST, implying that clustered vegetation lowers surface temperatures more effectively. In contrast, clustered spatial arrangements of anthropogenic land-cover types, especially impervious surfaces and open soil, elevate LST. These findings suggest that city planners and managers should, where possible, incorporate clustered grass and trees to disperse unmanaged soil and paved surfaces, and fill open unmanaged soil with vegetation. Our findings are in line with national efforts to augment and strengthen green infrastructure, complete streets, parking management, and transit-oriented development practices, and reduce sprawling, unwalkable housing development.

Key words: ASTER; daytime temperatures, nighttime temperatures; Las Vegas, Nevada, USA; local Moran's I; Phoenix, Arizona, USA; spatial autocorrelation; spatial configuration; urban landscape.

Introduction

The urban heat island (UHI) effect is a well-known phenomenon caused by urbanization. The process of replacing natural surfaces with manmade features significantly changes an area's energy balance and thermal properties. These changes are manifested in the area's land-surface temperatures (LST; Hart and Sailor 2009). Increased temperatures influence air quality, water consumption, and energy use. More importantly, anthropogenic changes can also increase the magnitude and duration of heat waves in cities, thereby elevating the risks of heat-related illnesses and deaths (Brazel et al. 2007). More heat-related illnesses and deaths are already expected to occur in the future due to a warming climate, population growth, and population aging (Sheridan et al. 2012, Hajat et al. 2014). Thus, it is important to implement effective strategies to

mitigate the UHI effect and avoid amplifying heat-related health outcomes.

The relationship between the composition of land cover and LST has been well established by previous studies (Weng et al. 2004, Yuan and Bauer 2007, Cao et al. 2010, Essa et al. 2013, Myint et al. 2013). These studies show that the percentage of green vegetation is negatively correlated with LST (Li et al. 2012, Myint et al. 2013, Zhou et al. 2014), while the percentage of impervious surfaces is positively correlated with LST (Yuan and Bauer 2007, Essa et al. 2013). Findings demonstrate that trees and other vegetative cover provide a cooling effect through evapotranspiration, effectively lowering summer LST when heat-related outcomes are at their peak. In contrast, impervious surfaces, such as building rooftops and pavements, elevate both day- and nighttime LST, with a stronger warming effect at night. Because of its effectiveness, increasing vegetative cover is one of the main strategies for reducing UHI.

High-resolution spatial imagery has not only opened up the possibility of studying detailed urban landscape impacts on LST, but also provided the capability to examine the spatial characteristics and arrangement of land-cover patches on LST. Many studies use the readily available land fragmentation metrics from the FRAG-STATS software (McGarigal and Marks 1995), such as patch density, edge density, patch cohesion, and landscape shape index, to examine the relationships between the spatial configuration of land-cover types and LST (Zhang et al. 2009, Li et al. 2011, Zhou et al. 2011, Connors et al. 2013, Kong et al. 2014, Maimai-tiyiming et al. 2014, Rhee et al. 2014). These studies found that land fragmentation has significant impacts on LST, indicating that spatial configuration can be optimized to mitigate the UHI effect. However, the land fragmentation metrics used in these studies, especially the metrics at the landscape level, which consider all patch types simultaneously, are not well designed to provide simple, direct interpretation or information on how to spatially design and arrange a specific land-cover type to achieve the most effective UHI mitigation.

For instance, Li et al. (2011) demonstrated positive correlations between LST and edge (patch) density and a negative relationship between LST and Shannon's diversity index (SHDI) at the landscape level. Their results suggest that several green-space patches provide a stronger UHI mitigation effect than when concentrated in a single area (Li et al. 2011). Zheng et al. (2014) examined the impacts of spatial configuration of paved surfaces on LST and found that clustered paved surfaces augment summer nighttime LST more severely than dispersed paved surfaces. Finally, another study by Zhou et al. (2011) reported that increases in edge density of woody and herbaceous vegetation decrease LST and that increases in shape complexity and variability of buildings and paved surfaces elevate LST. This study did not determine if interspersing vegetation evenly with buildings and paved surfaces could provide better cooling than grouping the vegetation relatively close together, because trees can be arranged spatially in various ways at the same edge-density level.

Configuration metrics often show good correlations with composition metrics (Riitters et al. 1995). Therefore, it is necessary to control for the effects of composition when examining the effects of land-cover type config-uration on LST. Furthermore, most studies did not consider landscape configurations as continuous surfac-es and calculated indices by tile or grid, resulting in a loss of information. One effective way to address these limitations is to use geostatistical techniques. Myint (2012) successfully employed a spatial autocorrelation index called Getis to examine the impacts of spatial configurations of green space on air temperature at 30-m resolution. Local Moran's I was also found effective for characterizing dispersed and clustered configurations of land-cover types, as it provides a continuous represen-tation of the true heterogeneity of the landscape (Fan and Myint 2014, Fan et al. 2015).

Given this background, this study aims to answers the following questions: (1) What are the relations between detailed urban land-cover types and surface tempera-tures in Las Vegas, Nevada, USA, in comparison to Phoenix, Arizona, USA? (2) Does the spatial arrange-ment of urban landscapes influence urban warming and cooling? (3) Are the impacts of spatial configuration on LST similar in magnitude for different land-cover types? (4) Is the type and level of relation between the spatial configuration of each land-cover type and LST different from one city to another? (5) Do spatial configurations of vegetation and built features still show similar impacts when other land-cover fractions are controlled?

Study Sites

Phoenix and Las Vegas are the cities observed in this study. These two subtropical desert climates have blistering-hot summers with daytime temperatures frequently exceeding 40°C. Because of these intense climate conditions, Phoenix and Las Vegas have serious water consumption and heat-related health issues (Myint et al. 2013). Both issues have been shown to be exacerbated by the UHI effect. Another important characteristic both urban metropolises share is their similar land-cover types. Grass, trees, paved and impervious surfaces, residential and commercial build-ings, and soil are the land-cover classes that were investigated for both cities in this study.

Data

The data used in this study include high-resolution multispectral satellite imagery for detailed urban land-cover mapping and thermal images for day- and
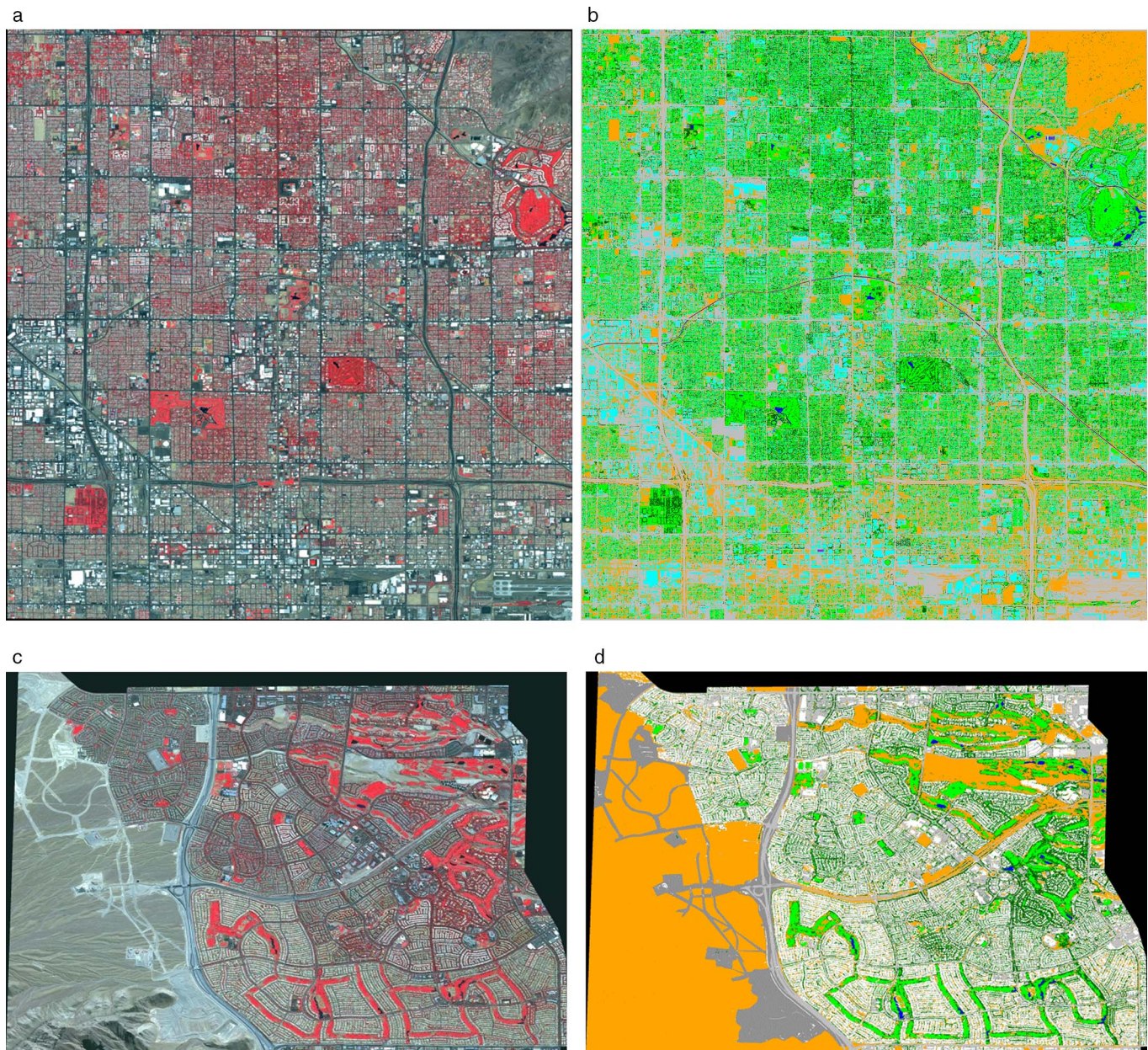
Fig. 1. (a) QuickBird image over Phoenix, Arizona, USA, (b) classified output of QuickBird, (c) Geoeye-1 image over Las Vegas, Nevada, USA (2011, DigitalGlobe; NextView license), and (d) classified output of Geoeye-1. For the classified panels, buildings are shown in cyan, trees/shrubs in dark green, grass in light green, unmanaged soil in orange, paved surfaces in gray, and water in blue.

nighttime surface temperature data over Phoenix and Las Vegas.

High-resolution satellite data and land-cover mapping

We employed two types of high-resolution satellite data; QuickBird imagery over Phoenix and Geoeye-1 (formerly Orbview 5) imagery over Las Vegas. The QuickBird image data over a central region in the city of Phoenix was acquired on 29 May 2007. The data set has a 2.4-m spatial resolution with four bands: blue (0.45–0.52 μm),

green (0.52–0.60 μm), red (0.63–0.69 μm), and near infrared (0.76–0.90 μm). The Geoeye-1 image was taken on 12 October 2011. The image has a 3-m spatial resolution with four bands: blue (0.45–0.51 μm), green (0.51–0.58 μm), red (0.66–69 μm), and near infrared (0.78–0.92 μm). Fig. 1 shows a subset of QuickBird and its output over Phoenix and Geoeye-1 and its output over Las Vegas.

To identify urban land-cover types in both Phoenix and Las Vegas, object-based image analysis (OBIA) was employed using the Definiens Developer software (Definiens, München, Germany). OBIA aggregates

Table 1. Producer's accuracies and user's accuracies for the land-cover maps generated from the QuickBird image over Phoenix, Arizona, USA, and Geoeye-1 (formerly Orbview 5) image over Las Vegas, Nevada, USA.

Cover type	Accuracy, Las Vegas		Accuracy, Phoenix	
	Producer (%)	User (%)	Producer (%)	User (%)
Soil	90.57	97.96	94.59	87.50
Impervious	90.24	90.24	83.65	98.86
Grass	82.50	97.06	95.77	79.07
Trees	82.86	76.32	86.15	84.85
Buildings	77.08	84.09	83.91	91.25
Pool	100.00	66.67	97.96	96.00
Water	100.00	96.67	100.00	100.00

Notes: The kappa coefficient was 0.87 for Las Vegas and 0.89 for Phoenix. Overall user's accuracy was 89.00% for Las Vegas and 90.40% for Phoenix.

Table 2. Area distribution and percent coverage of different land-cover types identified in the QuickBird imagery and Geoeye-1.

Land cover	Las Vegas		Phoenix	
	Area (km^2)	Cover (%)	Area (km^2)	Cover (%)
Soil	19.28	41.93	34.26	20.00
Impervious	7.81	16.99	43.13	25.18
Grass	2.81	6.11	40.12	23.42
Trees	5.67	12.32	18.86	11.01
Buildings	10.27	22.33	34.13	19.93
Pool	0.06	0.13	0.39	0.23
Water	0.09	0.19	0.00	0.00

pixels into discrete image objects based on their spectral and spatial characteristics (Blaschke and Strobl 2001). A set of decision rules was established to identify the various land-cover types, utilizing reflectance, PCA transformation values, vegetation indices, shape, and texture. To further refine the land-cover identification, the decision rules output was coupled with a nearest neighbor algorithm to produce the final land-cover map. The detailed classification procedure was presented in Myint et al. (2011). The identified urban land-cover types include buildings, trees/shrubs, grass, unmanaged soil, paved surfaces, pools, and open water. Swimming pools were excluded due to their small area coverage and because they do not have any considerable impact on nighttime temperatures, nor do they effectively lower thermal energy during the day in a desert environment (Myint et al. 2013).

To assess the accuracy of the classification, a stratified random sample approach was used (Congalton and Green 1999, Lillesand et al. 2008). References for validation included high-resolution imagery from Google Earth, the original image, ground survey, and local area knowledge. A total of 300 points with a minimum of 30 points per class were selected. Table 1 shows producer's accuracies, user's accuracies, the kappa coefficients, and overall accuracies for the land-cover maps generated from the QuickBird image over Phoenix and Geoeye-1 image over Las Vegas. The output maps for Las Vegas and Phoenix produced overall accuracies of 89.00% and 90.40%, respectively. Both output maps achieved overall accuracies of above 85%, which is the minimum mapping accuracy generally required for most mapping activities (Anderson et al. 1976). It can also be observed that both maps generated similar producers' and users' accuracies for all classes, which is also one of the key criteria for systematic land-use/land-cover (LULC) mapping (Lillesand et al. 2008). The area distribution and percent coverage of land-cover types in the two images are provided in Table 2.

ASTER surface temperatures

To examine day- and nighttime differences in LST, we used the Advanced Spaceborne Thermal Emission and Reflection Radiometer (ASTER) images at 90-m spatial resolution. For Las Vegas, ASTER summer daytime temperature data were acquired on 10 June 2011; nighttime temperature data were acquired on 17 October 2011. For Phoenix, one ASTER image was acquired during daytime on 6 July 2005; the nighttime image was acquired on 27 August 2005. ASTER provides more bands in the shortwave infrared (SWIR) and thermal infrared (TIR) range than other sensors, but at the same time, maintains a decent spatial resolution in the visible bands. In addition, the five TIR bands in ASTER represent LST more precisely and more accurate than other thermal sensors (Wan 1999, JPL 2001). We used the ASTER level-2 land-surface kinetic temperature product (i.e., ASTER08), which contains surface temperatures at 90-m resolution in degrees Kelvin, generated from the five TIR bands (Gillespie et al. 1999). For further analysis, the kinetic temperatures were converted into Celsius.

Weather conditions on the satellite acquisition dates

We examined the weather records for the six dates considered in this study using the NOAA NCEP archive (*available online*).[1] All six days were free of significant weather events. The 24-h cumulative precipitation was zero for all cases. Daily maximum and minimum air temperatures fell within the normal range (within one standard deviation) of the monthly statistics for the respective month and location. The maximum and minimum temperatures (temperature maximum and minimum) in °C for the six dates over the respective metropolitan areas were as follows: Phoenix, 29 May 2007 (37.8°, 22.2°), 6 July 2005 (44.4°, 27.8°), and 27 August 2005 (42.8°, 30.6°); Las Vegas, 12 October 2011 (28.3°, 16.7°), 10 June 2011 (35.0°, 22.8°), and 17 October

---

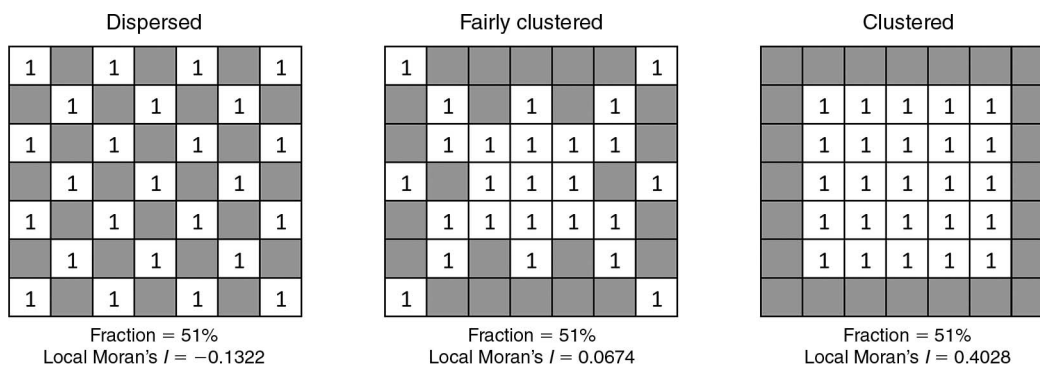[1] http://www.wpc.ncep.noaa.gov/dailywxmap

Fig. 2. Three hypothetical spatial configurations of a given land cover (e.g., grass, shown at 51% cover with a value of 1) in a 7 × 7 grid area, in association with other land-cover types (gray squares). Also shown are local Moran's *I* values.

2011 (34.4°, 20.6°). In summary, the synoptic conditions for the selected dates are representative of the seasonal conditions for the respective metropolitan areas in this study.

Methodology

First, the original resolution of the output fractions of each land-cover layer was aggregated to 90 m to match the spatial resolution of the ASTER image. Ordinary least squares (OLS) regression was used to understand the impacts of various urban land-cover types on LST in Las Vegas and Phoenix. We then constructed binary maps of buildings, trees, grass, unmanaged soil, paved surfaces, and water. For each binary map of a specific land-cover type, a value of one was assigned to pixels of the land-cover type and zero was assigned to pixels of other land-cover types.

We calculated local Moran's *I* for each binary map as a local indicator of spatial association (LISA) to characterize the spatial configuration (from clustered to dispersed) of urban landscapes at the local scale (Fan and Myint 2014). The index assesses the degree to which similar and dissimilar observation values cluster around interested locations (Anselin 1995). It is defined as

$$I_i(d) = \frac{x_i - \bar{x}}{\sum_i (x_i - \bar{x})^2} \sum_j w_{ij}(d)(x_j - \bar{x}) \qquad (1)$$

where x_i and x_j represent the attribute values (i.e., zero or one in the binary map) at locations i and j, $\bar{x}$ denotes the average attribute values for pixels in the entire image, and $\{w_{ij}(d)\}$ is a spatial weight matrix where the diagonal elements are all zero, and the off-diagonal elements are either one or zero, depending on whether the corresponding pixels are neighbors or not. The neighborhood was defined by the distance d.

The average local Moran's *I* values were normalized to the range of −1 to 1. Local Moran's *I* values of −1 represent highly dispersed configurations, values of zero indicate random configurations, and values of 1

represent highly clustered configurations. Fig. 2 shows hypothetical spatial configurations of a land-cover type (e.g., value 1 is grass) and their corresponding local Moran's *I* values. We computed local Moran's *I* values for every 90 × 90 m area to match the ASTER data.

To minimize the effects of land-cover composition on LST in the OLS regression, we further controlled for the land-cover composition by grouping observations with similar land-cover type fractions. Because it is impossible to obtain even a few observations with the same fractions for each land-cover type, we grouped the observations based on a 10% fraction range, yielding the following intervals: 0–9%, 10–19%, 20–29%, 30–39%, 40–49%, 50–59%, 60–69%, 70–79%, 80–89%, and 90–100%. A flow chart that demonstrates a step-by-step procedure to conduct this research study is presented in Fig. 3.

Results

Effects of land-cover fractions on LST

The relations between all types of land-cover fractions and day- and nighttime LST presented in Fig. 4 are statistically significant. Grass and trees were the two primary vegetated land-cover types observed. Both showed strong negative correlations with LST. Grass fractions for Phoenix during daytime ($r = 0.60$) and nighttime ($r = 0.63$) were found to have a stronger relationship with LST when compared to trees (Fig. 4). Although Phoenix trees had lower coefficients of determination for daytime ($r = 0.55$) and nighttime ($r = 0.40$), they did show steeper negative slopes (−16.29 daytime, −6.73 nighttime). This suggests that trees have a greater effect on lowering land-surface temperatures around them than grass. It is important to note here that LST from remote sensing reflects the canopy temperature and not the surface temperature under the tree where humans walk. At street level, heat is retained under and near tree canopies at night, especially in the winter, more than in open areas, due to reduced sky view factors and materials that turn cold quickly (i.e.,
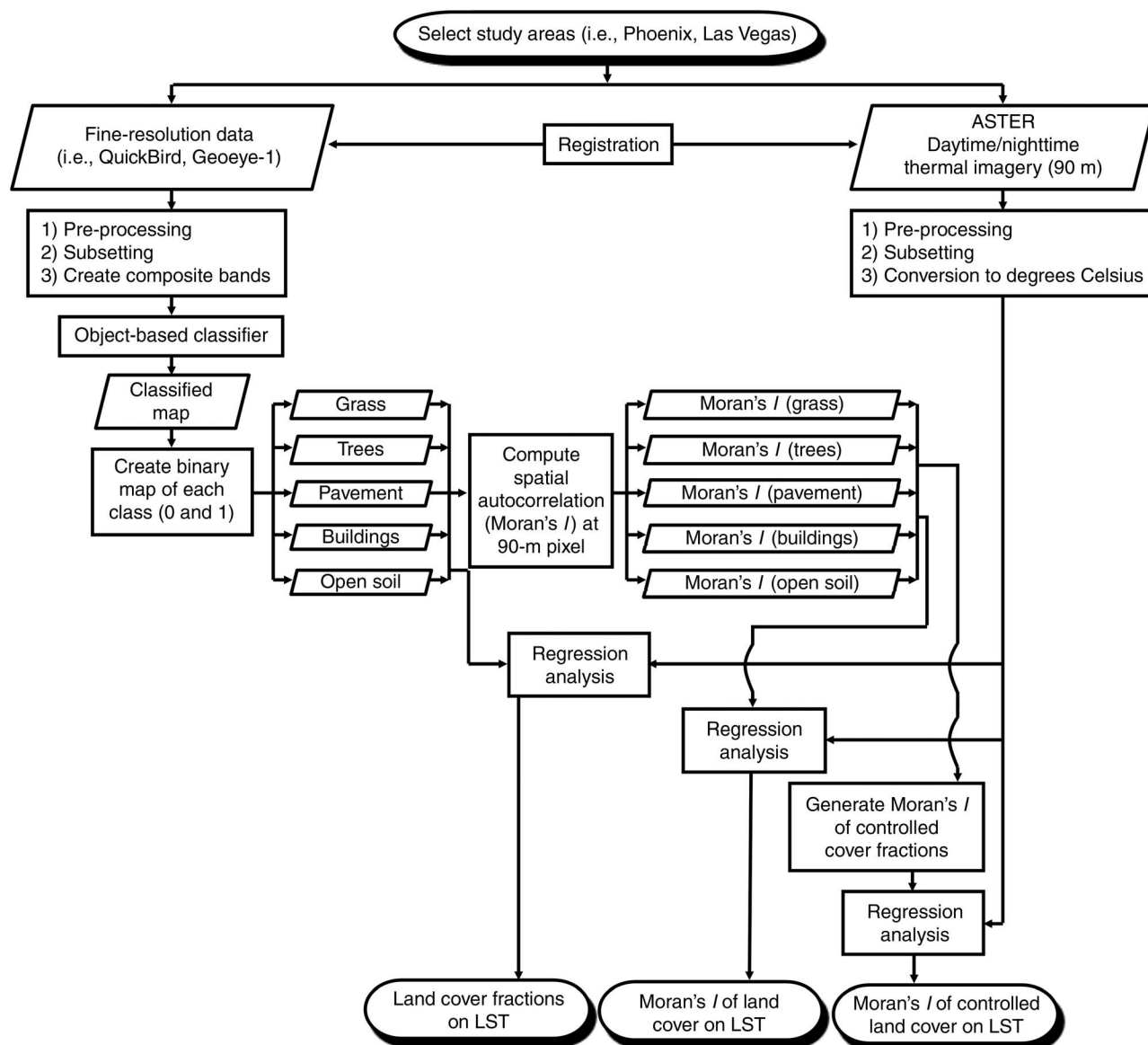
Fig. 3. Schematic of research design.

grass) when temperatures decrease. Unlike anthropogenic materials (e.g., metal, cement, asphalt) that retain heat, tree biomass (e.g., leaves, branches) does not hold heat. Helliker and Richter (2008) demonstrated that tree leaves manage to stay at an average temperature of 21.4°C over the course of a year regardless of the type of species and climate.

The same results were observed for Las Vegas, where daytime ($r = 0.61$) and nighttime ($r = 0.46$) grass fractions also showed stronger relationships with LST when compared to trees (Fig. 4). A notable difference here is the correlation coefficient for trees at daytime ($r = 0.40$) and nighttime ($r = 0.10$). One possible explanation for why trees in Las Vegas have little or no effect on lowering LST at night could be due to the location of the trees. The majority of trees and greenery in Las Vegas were located on the Strip, where hotels and other

commercial buildings can afford to place them out front. Because these trees are in such close proximity to and surrounded by paved surfaces, they may have little to no effect on lowering the already low early winter LST of anthropogenic covers at night. Also of note is that the nighttime ASTER image over Las Vegas was acquired in October when nighttime temperatures would have been relatively low in comparison to summer nights.

The other land types studied were paved surfaces, buildings, and soil. For Phoenix, paved surface fractions exhibited the strongest positive relationship with LST, with $r = 0.39$ for daytime and $r = 0.57$ for nighttime (Fig. 4). Paved surfaces showed a stronger relation with LST at night, most likely because asphalt retains heat during the day and slowly releases it after sunset. However, impacts on LST at day- and nighttime were similar. Soil in Phoenix also showed a positive correlation to LST, but
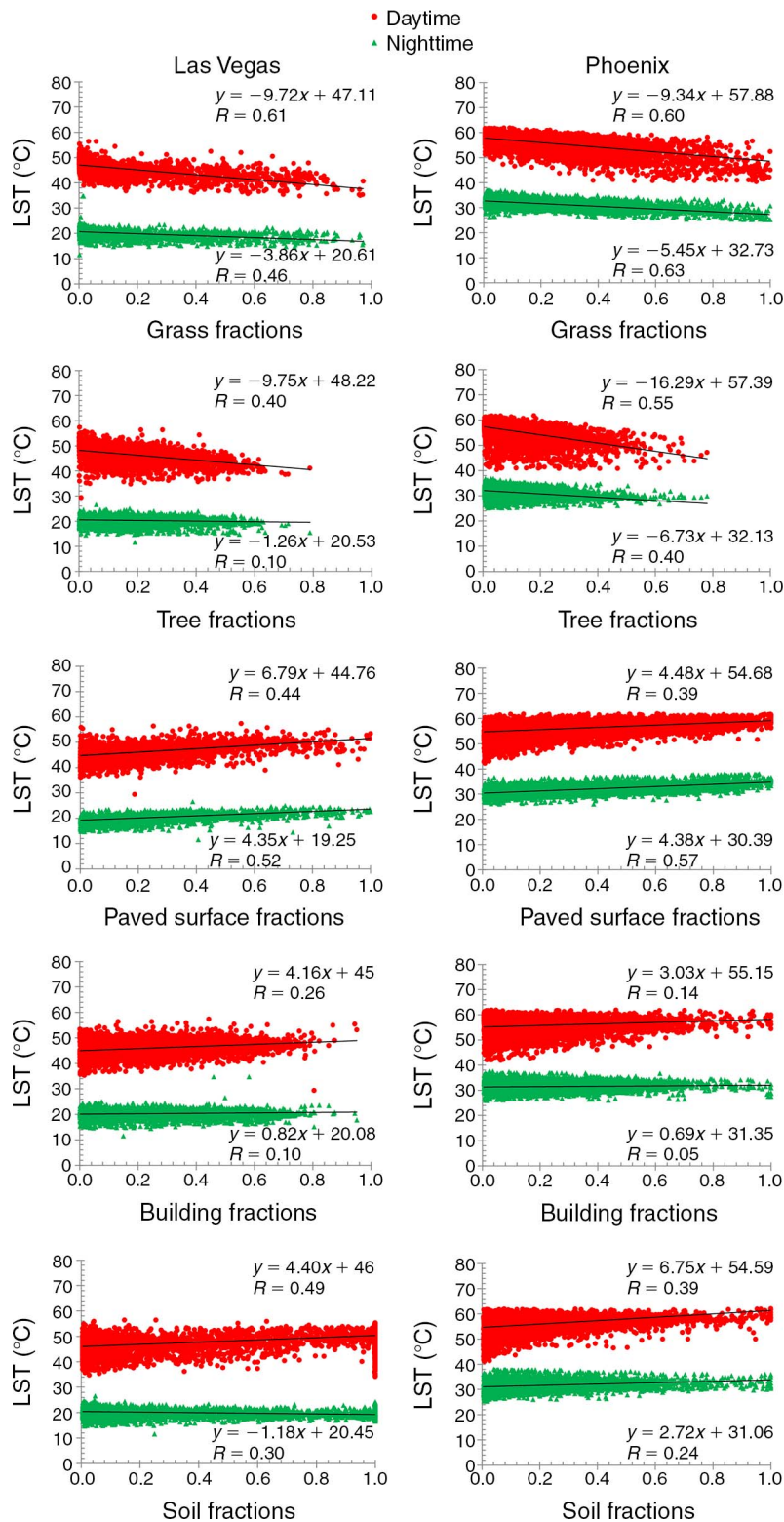
Fig. 4. Regression models and scatterplots of fractions of grass, trees, buildings, paved surfaces, and open soil vs. day- and nighttime land-surface temperature (LST) for Las Vegas and Phoenix ($P < 0.01$ for all regression models).

with weaker correlations for daytime ($r = 0.39$) and nighttime ($r = 0.24$). Paved surface fractions in Las Vegas revealed very similar results (Fig. 4). Even though the relation with daytime LST is lower ($r = 0.44$) than

nighttime LST ($r = 0.52$), the impact at daytime in Las Vegas is higher, since the regression's slope is steeper for daytime. Both relationships are statistically significant. Soil fractions in Las Vegas also have a positive

correlation to temperature, with daytime ($r = 0.49$) and nighttime ($r = 0.30$) yielding similar results to soil in Phoenix. Compared to paved surfaces, soil has a bigger impact on daytime temperatures in both cities.

In Phoenix, building fractions for daytime ($r = 0.14$) and nighttime ($r = 0.05$) showed very little or no positive correlation to LST. The same holds true for Las Vegas, where daytime ($r = 0.26$) and nighttime ($r = 0.10$) correlations were also low. The main reason for this weak relationship is that not every building structure interacts with its local environment in the same way. Residential homes in these areas, often only one to two stories high, yielded a positive relationship with LST in previous studies (Myint et al. 2013). These houses are usually covered with darker rooftop materials, which absorb more solar radiation. In addition, the lower height of these structures does not provide significant shade to cool the surrounding areas. Commercial buildings, on the other hand, often have the opposite effect on UHI; they can actually cool down their local environments (Myint et al. 2013), because these large buildings usually have high-albedo roofs that reflect sun radiation more efficiently and thus absorb less heat. During the daytime, commercial structures also provide large amounts of shade to areas directly around them, which reduces the amount of sun hitting surfaces, thus reducing the UHI. In addition, commercial buildings create a higher surface roughness than residential areas. This keeps cooler night air stored longer around high-rise buildings. Because of these differences in size, materials, and location between residential and commercial buildings, their overall relationship to LST is harder to determine due to mixed signals.

Effects of spatial configuration of land-cover types on LST

Local Moran's I was used to show the correlations between spatial configurations of the various land-cover types to LST. The relations between the local Moran's I of all land-cover types and day- and nighttime LST presented in Fig. 5 are statistically significant. For paved surfaces, buildings, and soils, there is a positive correlation between local Moran's I and LST, meaning as the type becomes more clustered (closer to 1), surface temperatures increase more. For the grass and tree types studied, a negative correlation between local Moran's I and LST was observed, implying that as these vegetation types become more clustered, LST decreases.

The spatial configuration of soil in Phoenix is positively correlated with LST daytime ($r = 0.42$) and nighttime ($r = 0.28$). In other words, temperatures are higher in areas where soil patches becomes more clustered. The same holds true for the daytime relationship in Las Vegas; however, for nighttime, our results show a negative correlation (an almost flat slope of -0.62), with $r = 0.32$. While this may have some

indirect implications, because both cities have a low correlation value for soil, it is not significant. For both cities, the spatial configuration of buildings shows a weak and nonsignificant positive correlation with LST for both day- and nighttime.

Grass and paved surfaces were the two land-cover types in both cities that showed strong correlations between spatial configuration and LST. Grass in Phoenix showed a negative correlation at daytime ($r = 0.64$) and nighttime ($r = 0.66$), with LST decreasing as the type becomes more clustered (Fig. 5). Grass in Las Vegas showed similar results, with a lower correlation coefficient at night ($r = 0.51$; Fig. 5). These results illustrate that as local Moran's I for grass gets higher (i.e., grass patches become more clustered), LST decrease. The inverse holds true for paved surfaces: as they become more clustered, LST increase. The spatial configuration of paved surfaces in both Phoenix and Las Vegas had strong positive correlations to surface temperatures with a stronger relationship at night.

Land-cover types naturally tend to cluster when fractions are increased and land-cover composition is not managed. Therefore, we observe grass and paved surfaces in groups, using the 10% fraction rule discussed previously. This allows us to control for land-cover composition. Our 9178 observations were segmented into 51 groups for grass and 59 groups for paved surfaces. Because the spatial configuration of grass has a stronger correlation to LST during the day, we only focus on these temperatures for Phoenix and Vegas (Tables 3 and 4). Since the correlation coefficients for the spatial configuration of paved surfaces are greater at night for both cities, only these temperatures are grouped.

All 51 groups for grass have statistically significant r values ($r > 0.30$). Out of the 12 medium to strong correlations observed, the most interesting group to note is the configuration 20–29% controlled grass with 10–19% trees, 10–19% impervious and soil, and 40–49% buildings (Phoenix). This is the lowest grass fraction group (<30% grass) that has a correlation greater than 0.45. Because of the high percentage of buildings in this specific group, this may indicate that the spatial configuration of grass can significantly impact LST near buildings.

Out of all high-correlation grass groups for both cities ($r > 0.40$), most fall into the 50–59% controlled grass range, with the exception of one group in Las Vegas. Out of these subgroups in Phoenix, the one with the most observations (165) has an r of 0.54. Here, grass fractions are 50–59%, trees 10–19%, soil and impervious 10–19%, and buildings 10–19%. In this group, local Moran's I values range from barely dispersed (-0.19) to somewhat clustered (0.42). This group is important, because it shows that as the fractions of all other land types remain constant, the spatial configuration of grass has a high correlation to LST with clustered configurations lower-
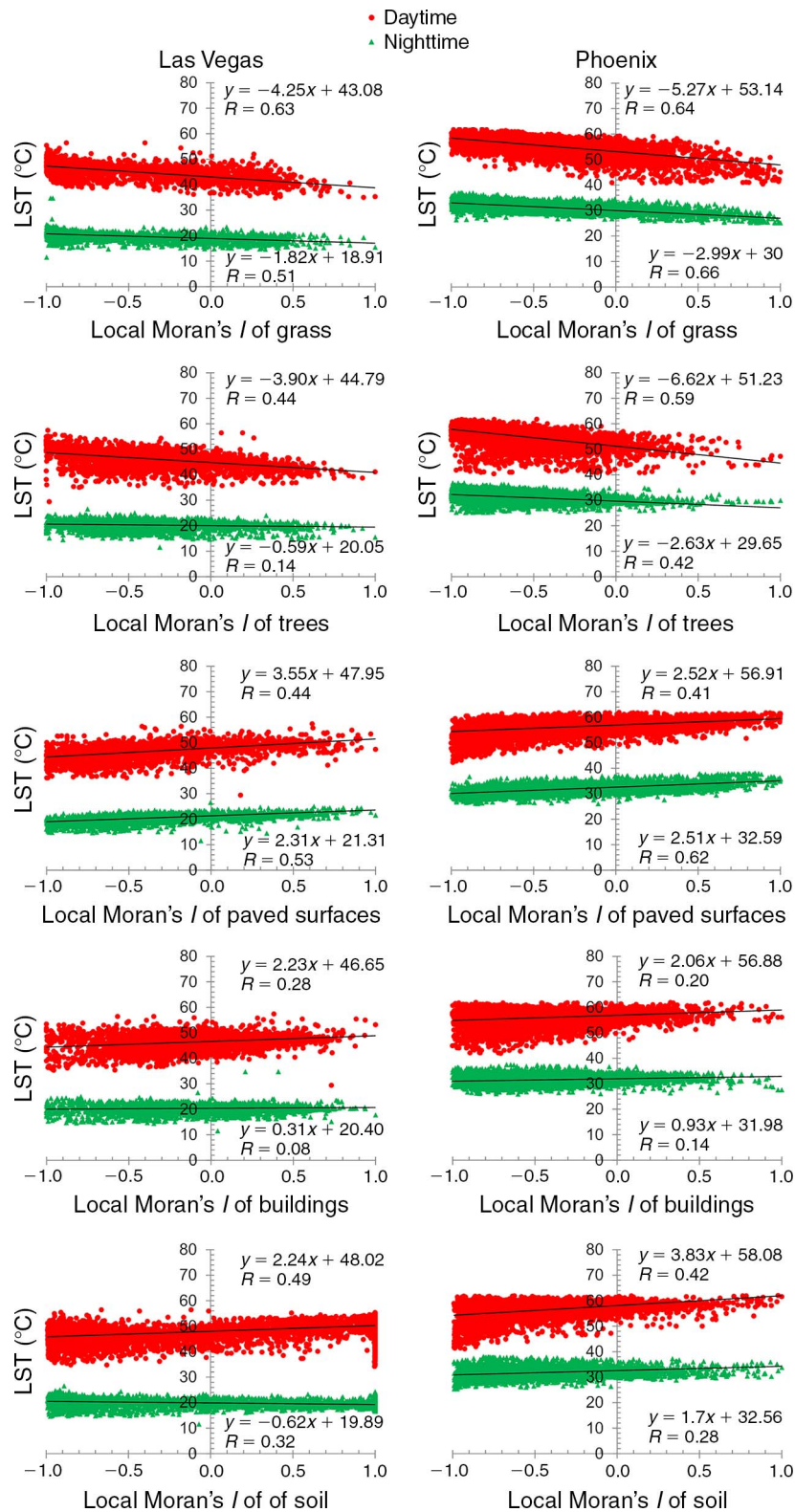
Fig. 5. Regression models and scatterplots of the spatial configuration (local Moran's *I*) of grass, trees, buildings, paved surfaces, and open soil vs. day- and nighttime LST for Las Vegas and Phoenix ($P < 0.01$ for all regression models).

ing temperatures more effectively.

The group with the strongest correlation ($r = 0.60$) was also found in Phoenix and had grass fractions of 50–59%, trees 20–29%, soil and impervious 0–9%, and

buildings 10–19%. Local Moran's *I* values here ranged from little dispersed (−0.14) to somewhat clustered (0.27). From this group's results, we can see that spatial configurations of grass (at daytime) have a significant

Table 3. Pearson correlation between local Moran's *I* of grass and daytime LST (land-surface temperature) under different controlled land-cover compositions (only those groups with *r* > 0.3), for Phoenix, Arizona, and Las Vegas, Nevada, USA.

Land-cover percentage					Moran's *I* for grass		Pearson correlation, Moran's *I* for grass and LST			
G	T	P + S	B	*n*	Min.	Max.	Slope	*r*	r^2	*P*
a) Phoenix										
10–19	0–9	20–29	50–59	32	−0.82	−0.34	−5.76	0.36	0.13	0.04
10–19	0–9	30–39	40–49	104	−0.81	0.25	−3.32	0.33	0.11	<0.01
10–19	0–9	80–89	0–9	55	−0.90	−0.10	−3.72	0.34	0.12	0.01
10–19	10–19	20–29	40–49	45	−0.82	−0.42	−9.51	0.33	0.11	0.02
10–19	10–19	60–69	0–9	95	−0.82	−0.29	−5.55	0.36	0.13	0.00
10–19	20–29	20–29	30–39	23	−0.75	−0.50	−10.17	0.36	0.13	0.07
10–19	20–29	40–49	10–19	50	−0.82	−0.37	−7.50	0.40	0.16	<0.01
10–19	20–29	50–59	0–9	22	−0.84	−0.35	−7.17	0.34	0.12	0.11
20–29	0–9	40–49	20–29	335	−0.72	0.12	−5.50	0.36	0.13	<0.01
20–29	0–9	50–59	10–19	244	−0.69	0.24	−5.19	0.40	0.16	<0.01
20–29	10–19	10–19	40–49	26	−0.59	−0.32	−10.79	0.47	0.22	0.02
20–29	10–19	40–49	20–29	230	−0.67	0.11	−5.97	0.35	0.12	<0.01
20–29	10–19	50–59	10–19	82	−0.72	−0.09	−5.65	0.36	0.13	<0.01
20–29	20–29	20–29	20–29	66	−0.67	−0.17	−6.88	0.33	0.11	0.01
30–39	0–9	20–29	30–39	121	−0.56	0.46	−6.30	0.33	0.11	<0.01
30–39	0–9	30–39	20–29	301	−0.54	0.12	−6.83	0.43	0.18	<0.01
30–39	0–9	40–49	10–19	144	−0.58	0.21	−5.79	0.45	0.20	<0.01
30–39	10–19	20–29	20–29	385	−0.51	0.03	−6.31	0.32	0.10	<0.01
30–39	10–19	40–49	10–19	87	−0.52	0.20	−6.23	0.34	0.12	<0.01
30–39	20–29	10–19	20–29	117	−0.47	−0.01	−7.80	0.31	0.10	<0.01
30–39	20–29	20–29	10–19	160	−0.46	−0.01	−10.13	0.41	0.17	<0.01
30–39	20–29	30–39	10–19	78	−0.50	0.15	−9.10	0.44	0.19	<0.01
30–39	30–39	10–19	10–19	86	−0.41	−0.02	−11.52	0.44	0.19	<0.01
30–39	40–49	10–19	0–9	27	−0.43	0.11	−9.00	0.50	0.25	0.01
40–49	0–9	30–39	10–19	78	−0.32	0.30	−4.08	0.35	0.12	<0.01
40–49	0–9	40–49	0–9	27	−0.35	0.34	−5.22	0.36	0.13	0.06
40–49	10–19	10–19	20–29	241	−0.11	0.15	−10.98	0.40	0.16	<0.01
40–49	10–19	20–29	10–19	383	−0.36	0.24	−7.21	0.34	0.12	<0.01
40–49	10–19	30–39	0–9	91	−0.35	0.32	−6.36	0.36	0.13	<0.01
40–49	20–29	0–9	20–29	52	−0.36	0.06	−11.65	0.41	0.17	<0.01
40–49	20–29	10–19	10–19	288	−0.37	0.24	−8.80	0.35	0.12	<0.01
40–49	20–29	20–29	0–9	113	−0.35	0.20	−6.72	0.31	0.10	<0.01
50–59	0–9	20–29	10–19	41	−0.15	0.37	−6.44	0.41	0.17	0.01
50–59	10–19	0–9	20–29	31	−0.17	0.28	−12.64	0.51	0.26	<0.01
50–59	10–19	10–19	10–19	165	−0.19	0.42	−12.60	0.54	0.29	<0.01
50–59	10–19	20–29	10–19	54	−0.12	0.27	−6.98	0.33	0.11	0.02
50–59	20–29	0–9	10–19	60	−0.14	0.27	−13.85	0.60	0.36	<0.01
50–59	20–29	10–19	0–9	85	−0.15	0.03	−10.34	0.37	0.13	<0.01
50–59	30–39	0–9	0–9	33	−0.12	0.31	−18.26	0.57	0.33	0.00
60–69	10–19	10–19	0–9	32	0.02	0.50	−11.11	0.38	0.15	0.03
60–69	20–29	0–9	0–9	36	0.03	0.60	−9.58	0.39	0.16	0.02
60–69	30–39	0–9	0–9	30	0.06	0.60	−17.33	0.40	0.16	0.03
70–79	0–9	10–19	0–9	26	0.17	0.67	−10.62	0.51	0.26	0.01
70–79	20–29	0–9	0–9	32	0.22	0.66	−17.64	0.46	0.21	<0.01
80–89	10–19	0–9	0–9	56	0.34	0.83	−10.89	0.43	0.18	<0.01
b) Las Vegas										
10–19	20–29	30–39	20–29	34	−0.82	0.09	−5.30	0.60	0.36	<0.01
10–19	30–39	20–29	20–29	28	−0.85	0.13	−3.05	0.37	0.14	0.05
20–29	20–29	20–29	20–29	20	−0.54	0.17	−3.61	0.36	0.13	0.11
30–39	20–29	10–19	20–29	15	−0.56	0.46	−5.14	0.47	0.22	0.08
70–79	10–19	0–9	0–9	28	0.15	0.61	−9.83	0.44	0.19	<0.01

Notes: Land covers shown are grass (G), trees (T), paved and soil together (P + S), and buildings (B). Statistics include number of samples (*n*), minimum (Min.) and maximum (Max.) values of local Moran's *I*, and regression slope, *r*, r^2, and *P* values. A *P* value of 0.06 was set as the threshold for significance in the regression models.

impact on LST when trees and buildings are the two other highest fractions. These results suggest that grass increases cooling, especially when located next to clustered buildings and trees, which provide a signifi-

cant amount of shade during the day.

More paved surface groups than grass groups were observed for both cities, with 25 groups for Las Vegas and 38 groups for Phoenix. All of the 59 paved surface

groups showed statistically significant correlations ($r >$ 0.30) between spatial configuration and LST. Twelve groups in Phoenix and nine in Las Vegas were found to have a medium to strong ($r > 0.40$) relationship between spatial configuration and nighttime LST. Of these 21 groups, 12 showed the strongest positive correlations ($r > 0.5$). In Phoenix, the highest correlation ($r = 0.71$) was found in the group with controlled paved surface fractions of 70–79%, vegetation (trees and grass) 0–9%, soil 20–29%, and buildings 0–9%. Local Moran's I values in this group ranged from barely clustered (0.18) to more packed (0.65). This group's high correlation suggests that the spatial configuration of paved surfaces has a large effect on LST when fractions of soil are second highest, indicating that if clustered paved surfaces share a plot of land with soil, LST are likely to be higher than if those paved surfaces were dispersed.

To solidify our conclusions, we look at another group from Phoenix, with paved surface fractions of 50–59%, green vegetation 0–9%, soil 40–49%, and buildings 0–9%. This group's observations ranged from barely dispersed (−0.09) to somewhat clustered (0.37). The high r value (0.53) of this group indicates that, once again, the spatial configuration of paved surfaces has a strong positive relationship with LST when sharing a plot of land with a high soil fraction, leading to increased nighttime temperatures.

Two groups, one in Phoenix ($r = 0.51$) and the other in Las Vegas ($r = 0.60$), showed strong spatial relationships to LST with paved fractions of only 20–29%. The group in Phoenix, ranging from highly dispersed (local Moran's I of −0.71) to barely scattered (local Moran's I of −0.15), also consists of vegetation fractions of 30–39%, soil 30–39%, and buildings 0–9%. As paved surfaces become less dispersed in this group, LST increases. For the Las Vegas group with paved surface fractions of 20–29%, greenery was 10–19%, soil was 20–29%, and buildings 30–39%. The observations in this group ranged from fairly dispersed (local Moran's I of −0.64) to almost random (local Moran's I of −0.09). The r value (0.60) here was one of the highest recorded, meaning that the spatial configuration of paved surfaces under this land composition has a very strong relationship to LST. As we can see, less-dispersed paved surfaces under these conditions increase LST.

Discussion

Effects of land-cover fractions on LST

Our findings show that different land-cover types have varying impacts on LST. Investigated separately, each observed type yielded a different day- and nighttime relationship to LST. Although results tended to be similar, each land-cover type also had varying impacts depending on the city.

Grass and tree fractions for Phoenix were negatively

correlated with LST, i.e., both types were effective in lowering surface temperatures. While trees were generally more effective in lowering daytime surface temperatures than nighttime temperatures in Las Vegas, they were much more effective in lowering LST during the day. Trees in Las Vegas hardly made any difference in LST at night ($r = 0.10$, slope $= -1.26$), possibly due to the warm air trapped in the tree biomass or high amounts of adjacent impervious surfaces that continue to release stored heat after sunset. On the other hand, trees (slope $= -16.29$) were more effective in lowering daytime LST than grass (slope $= -9.34$) in Phoenix, while grass (slope $= -9.72$) and trees (slope $= -9.75$) were equally effective in lowering daytime LST in Las Vegas. Paved surface increased LST in both Phoenix and Las Vegas, regardless of the time of day. Open soil (slope $= 4.40$ and 6.75 in Las Vegas and Phoenix, respectively) increased daytime LST more severely than buildings (slope $= 4.16$ and 3.03 in Las Vegas and Phoenix, respectively). Moreover, open soil in Phoenix (slope $= 6.75$) was more problematic than paved surfaces (slope $= 4.48$) in elevating daytime LST.

Effects of spatial configuration of land-cover types on LST

The spatial configurations of grass and trees in Las Vegas and Phoenix yielded strong negative relationships to LST. However, because the grass configurations had a greater relationship to LST than trees, we observed grass cover in groups and controlled for its land composition. We found that, with the remaining land-cover types held constant, grass decreased daytime LST significantly when clustered. In Phoenix particularly, grass lowered daytime surface temperatures more efficiently when it was less dispersed. From these results, it is recommended that city planners acknowledge the spatial importance of grass and trees compared to other land types and incorporate clustered vegetation accordingly.

The spatial configurations of buildings in both Phoenix and Las Vegas showed a weak relationship to daytime LST and an even weaker relationship to nighttime surface temperatures. However, the spatial configuration of buildings in Las Vegas seemed to show a greater impact on daytime LST than those in Phoenix. In other words, the denser buildings are arranged, the more concentrated shade they provide to paved surfaces throughout the day. It should be noted that temperatures of buildings represented rooftop temperatures in this study, and some buildings, especially in downtown commercial areas, may be cooler than their surrounding features due to height differences. Obviously, tearing down buildings and rebuilding them in ideal locations to provide shade is a poor option due to costs. Yet, measures can be taken to make existing buildings more cooling efficient. Alexandri and Jones (2008) found that the hotter and more arid a climate is, the greater the UHI mitigation effect of greenery attached to buildings and

Table 4. Pearson correlation between local Moran's *I* of paved surfaces and nighttime LST under different controlled land-cover compositions (only those groups with *r* > 0.3), for Phoenix, Arizona, and Las Vegas, Nevada, USA.

Land-cover percentage					Moran's *I* for paved surface		Pearson correlation Moran's *I* for paved surface and LST			
P	T + G	S	B	*n*	Min.	Max.	Slope	*r*	r^2	P
a) Phoenix										
10–19	0–9	30–39	40–49	21	−0.74	−0.27	4.49	0.45	0.20	0.04
10–19	0–9	40–49	30–39	21	−0.69	−0.08	3.49	0.37	0.14	0.10
10–19	0–9	50–59	20–29	19	−0.77	0.13	3.46	0.53	0.28	0.02
10–19	0–9	60–69	10–19	22	−0.77	−0.33	4.53	0.43	0.19	0.04
10–19	20–29	0–9	50–59	31	−0.76	0.18	2.84	0.43	0.18	0.02
10–19	20–29	10–19	40–49	48	−0.83	−0.15	5.14	0.48	0.23	<0.01
10–19	30–39	0–9	40–49	49	−0.81	−0.15	3.90	0.38	0.15	0.01
10–19	30–39	10–19	30–39	122	−0.81	−0.17	4.21	0.51	0.26	<0.01
10–19	40–49	20–29	10–19	245	−0.86	0.08	3.20	0.38	0.15	<0.01
10–19	50–59	20–29	10–19	58	−0.83	−0.16	3.40	0.36	0.13	<0.01
10–19	70–79	0–9	10–19	133	−0.85	0.18	2.84	0.34	0.12	<0.01
10–19	80–89	0–9	0–9	27	−0.68	−0.28	7.13	0.60	0.37	<0.01
20–29	10–19	40–49	10–19	72	−0.73	0.07	2.39	0.37	0.13	<0.01
20–29	20–29	0–9	40–49	43	−0.62	0.02	3.34	0.31	0.09	0.05
20–29	30–39	0–9	30–39	68	−0.69	−0.06	4.87	0.46	0.22	<0.01
20–29	30–39	10–19	20–29	198	−0.77	0.03	3.81	0.41	0.16	<0.01
20–29	30–39	20–29	10–19	135	−0.69	0.08	2.54	0.33	0.11	<0.01
20–29	30–39	30–39	0–9	36	−0.71	−0.15	5.04	0.51	0.26	<0.01
20–29	40–49	10–19	10–19	242	−0.77	0.06	2.48	0.33	0.11	<0.01
20–29	40–49	20–29	0–9	38	−0.71	0.03	3.71	0.39	0.15	0.01
20–29	50–59	10–19	0–9	78	−0.75	0.10	2.35	0.38	0.14	<0.01
30–39	20–29	30–39	0–9	41	−0.70	0.16	2.81	0.35	0.12	0.02
40–49	0–9	40–49	0–9	47	−0.31	0.21	2.82	0.33	0.11	0.02
40–49	0–9	50–59	0–9	25	−0.28	0.28	5.21	0.43	0.18	0.03
40–49	20–29	0–9	20–29	57	−0.37	0.19	3.76	0.39	0.16	<0.01
40–49	20–29	20–29	10–19	38	−0.38	0.24	4.28	0.48	0.23	<0.01
50–59	0–9	40–49	0–9	44	−0.09	0.37	6.00	0.53	0.29	<0.01
50–59	30–39	0–9	0–9	22	−0.19	0.36	3.02	0.38	0.15	0.08
60–69	0–9	20–29	0–9	73	0.01	0.55	3.56	0.30	0.09	0.01
60–69	0–9	30–39	0–9	47	0.06	0.60	6.53	0.47	0.22	<0.01
60–69	10–19	0–9	10–19	55	−0.03	0.48	3.74	0.32	0.10	0.02
70–79	0–9	0–9	10–19	126	0.07	0.67	4.46	0.42	0.17	<0.01
70–79	0–9	10–19	0–9	121	0.15	0.62	4.71	0.35	0.12	<0.01
70–79	0–9	20–29	0–9	59	0.18	0.65	11.61	0.71	0.50	<0.01
80–89	0–9	0–9	0–9	120	0.33	0.86	5.00	0.39	0.15	<0.01
80–89	0–9	10–19	0–9	76	0.34	0.85	11.26	0.66	0.44	<0.01

green roofs. Cool rooftop materials in combination with evapotranspiration from vegetation and increased shading effects could potentially make commercial buildings UHI-mitigation powerhouses.

Paved surfaces increased day- and nighttime temperatures significantly as their spatial configuration became more clustered. Paved surfaces include asphalt and other dark-colored impervious materials that release trapped heat at night. When these surfaces are clustered together, their warming effects are aggregated. Because spatial arrangements of paved surfaces had a large effect on LST at nighttime, we observed this land-cover type in groups and controlled for its land composition. Results showed that the clustering effect of paved surfaces most dramatically raised LST when combined near soil. These types of areas are usually large parking lots or highways surrounded by open soil.

Similar to paved surfaces, open soil elevated daytime LST more significantly than nighttime LST. The spatial configuration of soil in Phoenix and Las Vegas held a medium-to-high positive relationship to LST during the day and a weaker relationship at night. This means that clustered soil elevates surface temperatures more drastically during the daytime. It can be concluded that open soil should be dispersed around other land-cover types as much as possible or filled with vegetation in order to lower daytime LST and thus decrease the UHI.

This study shows that city planners and managers can help lower surface temperatures by clustering vegetation and trees together in between plots of paved surfaces. Another way to redesign these warm areas would be to add cool pavements. Our results also showed that the spatial configuration of paved surfaces in Las Vegas had a very strong positive relationship to nighttime LST when building fractions were high. Thus, clustered paved surfaces tend to increase nighttime LST

Table 4. Continued.

Land-cover percentage					Moran's *I* for paved surface		Pearson correlation Moran's *I* for paved surface and LST			
P	T + G	S	B	*n*	Min.	Max.	Slope	*r*	*r*^{2}	*P*
b) Las Vegas										
10–19	20–29	0–9	50–59	136	−0.79	−0.28	5.73	0.45	0.20	<0.01
10–19	20–29	10–19	40–49	58	−0.75	−0.34	5.34	0.37	0.14	<0.01
10–19	40–49	0–9	30–39	90	−0.77	−0.23	3.29	0.30	0.09	<0.01
20–29	0–9	10–19	50–59	18	−0.69	−0.29	5.58	0.55	0.30	0.02
20–29	10–19	0–9	40–49	30	−0.58	−0.24	5.64	0.39	0.15	0.03
20–29	10–19	10–19	40–49	40	−0.69	−0.08	2.51	0.32	0.10	0.04
20–29	10–19	0–9	50–59	166	−0.65	−0.15	4.26	0.37	0.14	0.00
20–29	10–19	10–19	50–59	44	−0.69	−0.21	2.90	0.31	0.10	0.04
20–29	10–19	0–9	60–69	40	−0.65	−0.22	5.99	0.53	0.28	<0.01
20–29	10–19	20–29	30–39	21	−0.64	−0.09	4.85	0.60	0.36	<0.01
20–29	20–29	0–9	40–49	199	−0.65	−0.05	4.03	0.36	0.13	<0.01
20–29	20–29	10–19	40–49	17	−0.60	−0.34	6.52	0.45	0.20	0.07
20–29	20–29	0–9	50–59	64	−0.65	−0.09	4.22	0.40	0.16	<0.01
20–29	30–39	10–19	20–29	20	−0.68	−0.19	4.17	0.39	0.15	0.09
20–29	30–39	0–9	30–39	131	−0.58	−0.25	4.04	0.35	0.12	<0.01
30–39	20–29	10–19	20–29	24	−0.50	0.20	4.12	0.49	0.24	0.01
30–39	30–39	0–9	30–39	42	−0.51	0.07	3.15	0.41	0.17	0.01
40–49	10–19	10–19	30–39	82	−0.39	0.42	2.19	0.39	0.15	<0.01
40–49	20–29	20–29	10–19	61	−0.36	0.23	2.73	0.40	0.16	<0.01
50–59	10–19	0–9	30–39	55	−0.12	0.49	2.46	0.35	0.12	0.01
60–69	20–29	0–9	10–19	22	0.11	0.51	7.65	0.50	0.25	0.02
70–79	0–9	0–9	10–19	22	0.34	0.76	7.93	0.47	0.22	0.03
70–79	10–19	0–9	0–9	15	0.33	0.78	4.95	0.61	0.37	0.02

Notes: Land covers shown are paved (P), trees and grass together (T + G), soil (S), and buildings (B). Statistics include number of samples (*n*), minimum (Min.) and maximum (Max.) values of local Moran's *I*, and regression slope, *r*, *r*^{2}, and *P* values. A *P* value of 0.06 was set as the threshold for significance in the regression models.

greatly when building percentages are also high, because these paved areas are less likely to receive shading during the day when commercial buildings are grouped closely together. If sidewalks, asphalt roads, and other paved materials are broken up by large patches of trees and/or grass, which provide shade and effectively lower LST through evapotranspiration, the UHI effect would be efficiently mitigated (Myint et al. 2013).

Conclusion

The purpose of this study was to understand the impacts of fractions of various land-cover types (both anthropogenic and natural) and their spatial configuration on LST in Phoenix and Las Vegas, as well as to compare these results in similar, yet distinct subtropical desert climates and urban areas. Findings confirmed our hypothesis that spatial configurations of land-cover types significantly influence LST.

We found that impervious materials, such as roads, parking lots, and driveways, had positive relationships with surface temperatures, raising LST as their percentages increased. Both vegetation types (grass and trees) had a negative correlation to LST, i.e., lowering surface temperatures as their percentages increased. In general, trees were found to lower LST slightly more effectively

than grass. Generally, buildings had a low positive or no relationship to LST. This result is consistent with a previous study by Myint et al. (2013) and suggests that buildings, especially commercial buildings with high-albedo roofs, actually reduce temperatures. This finding is not in line with the way urban planners traditionally think. It was found that most rooftops, especially commercial buildings, are composed of bright materials, leading to high reflectance and lower heat retention. Buildings increase surface roughness and may interact with surrounding materials, such as trees and grass, changing wind patterns. Finally, buildings provide shade almost the entire day, thereby providing a cooling effect similar to vegetation. The daytime cooling effect of dense urban forms was documented by several other studies (Pearlmutter et al. 1999, Middel et al. 2014).

Soil fractions in both cities significantly elevate LST, with higher impacts on daytime surface temperatures. Since soil has a significant impact on LST and can elevate daytime LST more than buildings, it is important that unmanaged soil or open land is filled with grass or trees to mitigate the UHI, especially when dealing with cities with hot climate conditions.

We believe that building sustainable cities is a must to achieve a sustainable world. Based on our results, it is recommended that policymakers, city managers, and urban planners incorporate and optimize the spatial

configuration of urban landscapes by clustering vegetation (i.e., grass, trees) and dispersing unmanaged soil and paved surfaces. While breaking up paved surfaces devoted to cars is likely to be beneficial, any attempt to keep buildings apart in an effort to mitigate urban warming effects will be counterproductive. It is especially important to consider the regional effects of spreading the built environment apart via increased vegetation, which can increase automobile dependence and decrease the viability of multimodal transportation, both of which have important implications for urban warming. It is most beneficial to insert vegetation and decrease paved surfaces in ways that augment and strengthen the national movements devoted to green infrastructure, complete streets, parking management, and transit-oriented development practices, while reducing urban sprawl and "unwalkable" housing developments.

Acknowledgments

Literature Cited

Alexandri, E., and P. Jones. 2008. Temperature decreases in an urban canyon due to green walls and green roofs in diverse climates. Building and Environment 43:480–493.

Anderson, J., E. E. Hardy, J. T. Roach, and R. E. Witmer. 1976. A land use and land cover classification system for use with remote sensor data. Geological Survey professional paper 964. United States Government Printing Office, Washington, D.C., USA.

Anselin L. 1995. Local indicators of spatial association—LISA. Geographical Analysis 27:93–115.

Blaschke, J., and J. Strobl. 2001. What's wrong with pixels? Some recent developments interfacing remote sensing and GIS. GIS–Zeitschrift für Geoinformationssysteme 14:12–17.

Brazel, A., P. Gober, S. J. Lee, S. Grossman-Clarke, J. Zehnder, B. Hedquist, and E. Comparri. 2007. Determinants of changes in the regional urban heat island in metropolitan Phoenix

(Arizona, USA) between 1990 and 2004. Climate Research 33:171–182.

Cao, X., A. Onishi, J. Chen, and H. Imura. 2010. Quantifying the cool island intensity of urban parks using ASTER and IKONOS data. Landscape and Urban Planning 96:224–231.

Congalton, R. G., and K. Green. 1999. Assessing the accuracy of remotely sensed data: principles and practices. Lewis, Boca Raton, Florida, USA.

Connors, J., C. Galletti, and W. L. Chow. 2013. Landscape configuration and urban heat island effects: assessing the relationship between landscape characteristics and land surface temperature in Phoenix, Arizona. Landscape Ecology 28:271–283.

Essa, W., J. van der Kwast, B. Verbeiren, and O. Batelaan. 2013. Downscaling of thermal images over urban areas using the land surface temperature–impervious percentage relationship. International Journal of Applied Earth Observation and Geoinformation 23:95–108.

Fan, C., and S. Myint. 2014. A comparison of spatial autocorrelation indices and landscape metrics in measuring urban landscape fragmentation. Landscape and Urban Planning 121:117–128.

Fan, C., S. Myint, and B. Zheng. 2015. Measuring the spatial arrangement of urban vegetation and its impacts on seasonal surface temperatures. Progress in Physical Geography 39:199–219.

Gillespie, A. R., S. Rokugawa, S. J. Hook, T. Matsunaga, and A. B. Kahle. 1999. Temperature/emissivity separation algorithm theoretical basis document. Version 2.4. NASA, Washington, D.C., USA. http://eospso.gsfc.nasa.gov/eos_homepage/for_scientists/atbd/docs/ASTER/atbd-ast-05-08.pdf

Hajat, S., S. Vardoulakis, C. Heaviside, and B. Eggen. 2014. Climate change effects on human health: projections of temperature-related mortality for the UK during the 2020s 2050s and 2080s. Journal of Epidemiology and Community Health 68:641–648.

Hart, M., and D. Sailor. 2009. Quantifying the influence of land-use and surface characteristics on spatial variability in the urban heat island. Theoretical and Applied Climatology 95:397–406.

Helliker, B. R., and S. L. Richter. 2008. Subtropical to boreal convergence of tree-leaf temperatures: an isotopic analysis. Nature 454:511–514.

JPL [Jet Propulsion Laboratory]. 2001. ASTER higher-level product user guide, advanced spaceborne thermal emission and reflection radiometer. Jet Propulsion Laboratory, California Institute of Technology, La Cañada Flintridge, California, USA. http://asterweb.jpl.nasa.gov/content/03_data/04_Documents/ASTERHigherLevelUserGuideVer2May01.pdf

Kong, F., H. Yin, P. James, L. C. Hutyra, and H. S. He. 2014. Effects of spatial pattern of green space on urban cooling in a large metropolitan area of eastern China. Landscape and Urban Planning 128:35–47.

Li, J., C. Song, L. Cao, F. Zhu, X. Meng, and J. Wu. 2011. Impacts of landscape structure on surface urban heat islands: a case study of Shanghai, China. Remote Sensing of Environment 115:3249–3263.

Li, X., W. Zhou, Z. Ouyang, W. Xu, and H. Zheng. 2012. Spatial pattern of greenspace affects land surface temperature: evidence from the heavily urbanized Beijing metropolitan area China. Landscape Ecology 27:887–898.

Lillesand, T., R. W. Kiefer, and J. Chipman. 2008. Remote sensing and image interpretation. Sixth edition. John Wiley & Sons, Hoboken, New Jersey, USA.

Maimaitiyiming, M., A. Ghulam, T. Tiyip, F. Pla, P. Latorre-Carmona, Ü. Halik, M. Sawut, and M. Caetano. 2014. Effects of green space spatial pattern on land surface temperature: Implications for sustainable urban planning and climate change adaptation. ISPRS Journal of Photogrammetry and

Remote Sensing 89:59–66.

McGarigal, K., and B. J. Marks. 1995. FRAGSTATS: spatial pattern analysis program for quantifying landscape structure. General technical report PNW-GTR-351. USDA Forest Service, Pacific Northwest Research Station, Portland, Oregon, USA.

Middel, A., K. Häb, A. J. Brazel, C. A. Martin, and S. Guhathakurta. 2014. Impact of urban form and design on mid-afternoon microclimate in Phoenix local climate zones. Landscape and Urban Planning 122:16–28.

Myint, S. W. 2012. Advances in mapping from aerospace imagery. Pages 261–278 in X. Yang and J. Li, editors. Advances in mapping from remote sensor imagery: techniques and applications. CRC Press, Boca Raton, Florida, USA.

Myint, S. W., P. Gober, A. Brazel, S. Grossman-Clarke, and Q. Weng. 2011. Per-pixel versus object-based classification of urban land cover extraction using high spatial resolution imagery. Remote Sensing of Environment 115:1145–1161.

Myint, S. W., E. Wentz, A. J. Brazel, and D. A. Quattrochi. 2013. The impact of distinct anthropogenic and vegetation features on urban warming. Landscape Ecology 28:959–978.

Pearlmutter, D., A. Bitan, and P. Berliner. 1999. Microclimatic analysis of "compact" urban canyons in an arid zone. Atmospheric Environment 33:4143–4150.

Rhee, J., S. Park, and Z. Lu. 2014. Relationship between land cover patterns and surface temperature in urban areas. GIScience and Remote Sensing 51:521–536.

Riitters, K. H., R. V. O'Neill, C. T. Hunsaker, J. D. Wickam, D. H. Yankee, S. P. Timmins, K. B. Jones, and B. L. Jackson. 1995. A factor analysis of landscape pattern and structure metrics. Landscape Ecology 10:23–39.

Sheridan, S., M. Allen, C. Lee, and L. Kalkstein. 2012. Future heat vulnerability in California. Part II: projecting future heat-related mortality. Climatic Change 115:311–326.

Wan, Z. 1999. MODIS land-surface temperature algorithm theoretical basis document (LST ATBD). Institute for Computational Earth System Science, University of California, Santa Barbara, California, USA. http://modis.gsfc.nasa.gov/data/atbd/atbd_mod11.pdf

Weng, Q., D. Lu, and J. Schubring. 2004. Estimation of land surface temperature–vegetation abundance relationship for urban heat island studies. Remote Sensing of Environment 89:467–483.

Yuan, F., and M. E. Bauer. 2007. Comparison of impervious surface area and normalized difference vegetation index as indicators of surface urban heat island effects in Landsat imagery. Remote Sensing of Environment 106:375–386.

Zhang, X., T. Zhong, X. Feng, and K. Wang. 2009. Estimation of the relationship between vegetation patches and urban land surface temperature with remote sensing. International Journal of Remote Sensing 30:2105–2118.

Zheng, B., S. W. Myint, and C. Fan. 2014. Spatial configuration of anthropogenic land cover impacts urban warming. Landscape and Urban Planning 130:104–111.

Zhou, W., G. Huang, and M. L. Cadenasso. 2011. Does spatial configuration matter? Understanding the effects of land cover pattern on land surface temperature in urban landscapes. Landscape and Urban Planning 102:54–63.

Zhou, W., Y. Qian, X. Li, W. Li, and L. Han. 2014. Relationships between land cover and the surface urban heat island: seasonal variability and effects of spatial and thematic resolution of land cover data on predicting land surface temperatures. Landscape Ecology 29:153–167.